HHS Public Access

Author manuscript

J Phys Chem B. Author manuscript; available in PMC 2018 May 11.

Published in final edited form as:

J Phys Chem B. 2017 May 11; 121(18): 4799–4809. doi:10.1021/acs.jpcb.7b02468.

Beyond Structural Biology to Functional Biology: Solid-State NMR Experiments and Strategies for Understanding the M2 Proton Channel Conductance

Huajun Qin[1,⊥], **Yimin Miao**[1,⊥], **Timothy A. Cross**[1,2], and **Riqiang Fu**[2,*]

[1]Department of Chemistry and Biochemistry, Florida State University, Tallahassee, Florida 32306, USA

[2]National High Magnet Field Lab, 1800 East Paul Dirac Drive, Tallahassee, Florida 32310, USA

Abstract

In terms of structural biology, solid-state NMR experiments and strategies have been well established for resonance assignments leading to the determination of three-dimensional structures of insoluble membrane proteins in their native-like environment. It is also known that NMR has the unique capabilities to characterize structure-function relationships of membrane-bound biological systems beyond structural biology. Here, we report on solid-state NMR experiments and strategies for extracting functional activities on a sub-msec time scale. Specifically, we use the His37-labeled full length M2 (M2FL) protein of *Influenza A* virus embedded in synthetic lipid bilayers as an example to characterize the proton conduction mechanism and kinetics. The integral membrane M2 protein assembles as a tetrameric bundle to form a proton-conducting channel that is activated by low pH and is essential for the viral lifecycle. Our results present convincing evidence for the formation of imidazolium-imidazole hydrogen-bonds in the His37 tetrad at low pH and that these hydrogen bonds have a low barrier that facilitates the proton conduction mechanism in the M2FL protein. Moreover, it has been possible to measure hydronium ion exchange between water and the protons in the His37 NH bonds based on chemical exchange spectroscopy with minimized spin diffusion. The results identify an exchange rate constant of ~4000 s^{-1} for pH 5.8 at −10°C.

TOC image

Corresponding author: R. Fu, rfu@magnet.fsu.edu.

⊥These authors contributed equally.

Supporting Information. Controlled ^{13}C-^{13}C and ^{15}N-^{15}N correlation spectra for chemical exchange spectroscopy; 1D ^{15}N spin-echo spectra of the His37-labeled M2FL (pH 5.8) and the T_2 fittings; $T_{1\rho}^{H}$ measurements.

Notes

The authors declare no competing financial interest.

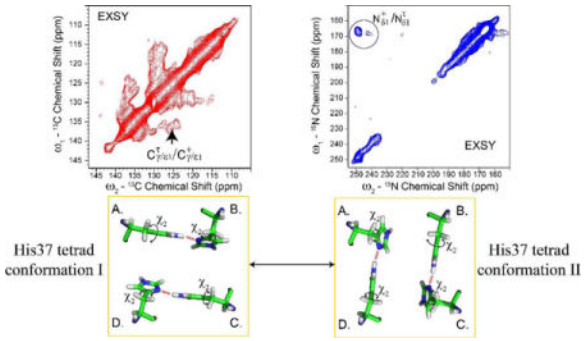

1. INTRODUCTION

One of the major frontiers in structural biology is membrane proteins, whose structure, dynamics and function are different from water-soluble proteins. They exist in a heterogeneous lipid bilayer environment exhibiting diverse conformations and conduct many essential biological processes, such as inter- and intra-cellular signal transduction, protein localization, and trafficking requiring synergistic effects between the proteins and their surrounding complex environments[1–3]. In the past decades, high-resolution solid-state magic-angle-spinning (MAS) NMR has become a proven powerful technique for characterizing these insoluble membrane proteins and their interactions with the lipid environs[4–9]. From a structural biology point of view, an assignment of resonances is mandatory in order to precisely determine high-resolution three-dimensional protein structures. However, spectral resolution in these proteins is a major hurdle because of the uniform low dielectric environment in the transmembrane (TM) domain that often yields highly uniform helical structure resulting in very little chemical shift dispersion. The high hydrophobic amino acid content can yield significant tertiary structural heterogeneity and the hydrophilic content can lead to multiple interactions with the heterogeneous lipid interface resulting in opportunities for exchange dynamics, which can broadens resonances. In the sample preparation for structural biology the interactions with various membrane mimetic environments can lead to spectral differences in the structural models generated[10–13].

Nevertheless, adapting the concepts used in solution[14], solid-state MAS NMR experiments and strategies for the resonance assignments, an essential step towards structural determination of uniformly ^{15}N and ^{13}C labeled proteins, have been well established[15], routinely requiring multi-dimensional solid-state MAS NMR techniques: 1) identifying ^{13}C resonances of all amino acid types based on homo-nuclear ^{13}C-^{13}C correlation[16–22]; 2) obtaining intra-residue assignment of ^{15}N resonances via NCA experiments; 3) establishing inter-residue sequential assignments[15, 23–26] to neighboring residues through $N_i(CO)_{i-1}$, $N_{i+1}(CO)CA_i$, or $CA_i(CO)N_{i+1}$, due to the fact that the backbone nitrogen of residue i covalently bonds with the carbonyl (C′) carbon of residue i-1 and the Cα of residue i providing a through-bond linkage between two sequential residues. Often, three-dimensional experiments, in a combined use of the above experiments, such as NCOCX and NCACX[27] are performed in order to improve the spectral resolution. In addition, long-range inter-residue interactions are required to provide structural long-range distance restraints, often

achieved by homo-nuclear ^{13}C-^{13}C correlation experiments with long mixing times. Difference spectroscopy[28] has been proposed to subtract the spin diffusion resonances of relatively short intra-residue distances from the longer inter-residue distances, leading to a better identification of the inter-residue resonances in crowded two-dimensional (2D) ^{13}C-^{13}C chemical shift correlation spectra intrinsically associated with a long mixing time. Similarly, relaxation-compensated difference spin diffusion NMR[29] is also used to detect the long-range correlations. As NMR has the unique capabilities to characterize proteins with dynamic domains in native-like environments, the question is how to extract the functional information beyond the structural information. Here, we illustrate solid-state NMR experiments and strategies aimed at obtaining dynamics and exchange kinetics for proton channel conductance using the *Influenza A* full length M2 protein (M2FL) as an example.

The M2 protein is a 97-residue membrane protein with a 22-residue N-terminal and a 51-residue C-terminal segment connected by a single TM helix of 24 residues. It assembles as a tetrameric bundle to form a proton-conducting channel functioning at a slow rate (10^2–10^3/s) that is activated by low pH and is essential for the viral lifecycle[30, 31]. The α-helical TM tetramer (residues 25–46) is responsible for the proton conductance that triggers the release of viral RNA into the host cells. This tetrameric TM domain is an important drug target[32–35]. The four His37 residues reside near the center of the TM helix and are known to be the heart of the proton conducting channel, the key to the mechanism of proton transport[36]. To the C terminus of the TM helix is an amphipathic helix (residues 47–62)[37–39] that has been shown to interact with the interfacial region of the lipid bilayer and is believed to be essential for membrane trafficking, localization and viral budding[40, 41]. So far, several different constructs reconstituted in various lipid environments have been the subject to intensive structural studies in the past decade using both MAS[42–49] and oriented sample[32, 50–53] solid-state NMR, as well as solution NMR[37, 54–56] and x-ray crystallography[57, 58]. It has been found that spectra from M2 vary dramatically depending on the M2 constructs and membrane mimetic environments used in the reconstitution, especially those associated with the conductance mechanism[49, 59–62], thus leading to different proton transfer mechanisms. For the conductance domain M2(22–62) in DOPC/DOPE lipids[43] and M2(18–60) in POPC and DPhPC[46–49], as well as for the M2FL protein in both DOPC/DOPE lipids and *E. coli* membranes[42], a set of two ^{13}C resonances for His37 was observed, suggesting the histidine tetrad exhibits a dimer of dimer conformation. Recently, in the pH titration study of the M2FL including ^{15}N, ^{15}N-^{13}C and ^{13}C-^{13}C spectra of liquid crystalline lipid bilayer preparations, the derived first two pKa's have identical values of 6.3±0.1, which were significantly lower than those obtained from different M2 constructs[36, 48, 49, 59, 63]. Furthermore, the ^{1}H-^{15}N heteronuclear correlation (HETCOR) spectra of the His37 sidechains show that the ^{15}N resonances spread from 165 to ~200 ppm while their correlated ^{1}H frequencies extend up to 19 ppm[60]. Such high ^{15}N and ^{1}H frequencies conclusively indicate the formation of short imidazole-imidazolium H-bonds[64] in the histidine tetrad at low pH. This confirms the model of the so-called low-barrier hydrogen bond (LBHB), i.e., where the shared proton can transit across the potential energy barrier within each pair of His37 residues[36, 51, 60]. One-dimensional (1D) pure chemical exchange measurements proposed recently[65] also confirm that the hydronium ions are in exchange with protons in

the His37 NH bonds at the heart of the M2 proton conduction mechanism, with an exchange rate constant of ~1750 s^{-1} at pH 6.2 and −10°C.

On the other hand, the M2 TM domain M2(22–46) in a virus-envelope-mimetic lipid membrane shows quite a different set of His37 resonances[63] that does not support amantadine binding. In the ^{1}H-^{15}N HETCOR spectra of this preparation at a similar pH[61], the ^{15}N peaks were in the range of 160–180 ppm, correlating to ^{1}H chemical shifts of 8–12 ppm, similar to the backbone amide ^{1}H chemical shift range. No imidazole-imidazolium cross peaks were observed in the ^{13}C-^{13}C correlation spectra of the +2 charged channel state[63]. Therefore, an alternative proton conducting mechanism[28,29] with the His37 shuttling protons through imidazole ring reorientations and exchanging protons with water, without forming any inter-monomer hydrogen bond between the His37 residues[61, 63] was proposed. It is noteworthy that the inclusion of the cytoplasmic tail in the M2 construct (residues 21–97) in the virus-envelope-mimetic lipid membrane binds amantadine[59]. Recently, it has also been shown that cholesterol stabilizes the amphipathic helix in the lipid interface[66].

Slow chemical exchange and spin diffusion are two main mechanisms that result in cross-peaks in homonuclear chemical shift correlation experiments. Chemical exchange represents kinetic processes within the molecules and can only be manipulated by temperature, not by any experimental techniques. The buildup of the cross-peak intensities in the exchange spectroscopy (EXSY)[67] solely depends on the chemical exchange rate constant. On the other hand, spin diffusion is primarily dependent upon the strength of through-space homo-nuclear dipolar interactions (proportional to $1/r^6$, where r is the distance between the two spins)[68]. However, when spin diffusion is mediated by abundant spins (e.g. protons), such as in proton driven spin diffusion (PDSD)[68] and the rotary resonance conditions[17, 19, 20, ^{13}C-^{13}C spin diffusion is greatly enhanced and consequently becomes one of the most useful tools for obtaining homonuclear ^{13}C-^{13}C chemical shift correlation spectra, an important building block for obtaining carbon-carbon distance restraints for protein structural elucidation. Typically, a short mixing time (such as a few milliseconds) can generate cross peaks between directly bonded carbons to establish the intra-residue connectivity. Therefore, the chemical exchange information is severely buried in the ^{13}C-^{13}C correlation spectra. Here, we will use uniformly ^{13}C,^{15}N-labeled M2FL protein at pH 5.8 to demonstrate how to minimize spin diffusion induced cross peaks so that the chemical exchange induced imidazole-imidazolium cross peaks from the His37 tetrad could be observed in the homonuclear correlation spectra. We will then summarize our recent experiments to analyze the dynamic process in this sample.

2. EXPERIMENTAL METHODS

Protein expression, purification and reconstitution

M2FL ($H_{57,90}Y$) protein expression, purification and reconstitution in DOPC/DOPE liposomes are detailed in the literature[28, 60]. It is important to note that in the uniform ^{13}C and ^{15}N labeling media for protein expression, unlabeled Phe, Tyr, and Trp amino acids were added to the bacterial cultures to suppress all of the aromatic amino acid resonances except those from the His37 tetrad.

Solid-State NMR Spectroscopy

The proteoliposome pellet containing approximately 10 mg of the M2FL protein was packed into a 3.2-mm thin-wall rotor (36 μL sample volume). Figure 1 shows the pulse sequence for 2D homo-nuclear correlation experiments with various irradiation schemes (PARIS[19], no irradiation, and high power ^{1}H SPINAL64 decoupling[69]) during the mixing time. The 2D ^{13}C-^{13}C correlation spectra and 1D ^{15}N spin-echo spectra were acquired on a Bruker Avance 600.1 MHz NMR spectrometer using an NHMFL 3.2 mm Low-E triple-resonance biosolids MAS probe[70, 71]. The sample spinning rate was controlled by a Bruker pneumatic MAS unit at 12.2 kHz ± 3Hz. The ^{13}C magnetization was enhanced by cross polarization (CP) with a contact time of 1 ms, during which a ^{1}H spin-lock field of 50.0 kHz was used and the ^{13}C B_1 field was ramped from 38 to 56 kHz[72]. The ^{13}C 90° pulse length was 3.0 μs. A SPINAL64 decoupling sequence[69] with an ^{1}H B_1 field of 78.0 kHz was used during the t_1 and t_2 dimensions. TPPI was used for quadrature detection in the t_1 dimension[73]. During the mixing time of t_m=20 ms, 12.2 and 78.0 kHz ^{1}H B_1 fields were applied for the PARIS and SPINAL64 irradiation, respectively. The acquisition times for the t_1 and t_2 dimensions were 4.53 and 7.74 ms, respectively. The data were zero-filled to a 4096 × 2048 matrix before Fourier transform and were processed with a Gaussian window function (LB=−50 Hz and GB=0.1) in both dimensions. 1D ^{15}N spin-echo spectra were acquired with a Lee-Goldburg (LG) cross polarization (LGCP) sequence[74] using the contact time of 4 ms, during which the ^{1}Hs were spin-locked along the magic angle by the LG sequence. The ^{15}N 180° pulse length was 8.2 μs and the echo time was set to a multiple of the spinning periods. A SPINAL64 decoupling sequence[69] with a ^{1}H B_1 field of 78.0 kHz was applied during the spin echo and data acquisition times.

The 2D ^{15}N-^{15}N and ^{1}H-^{15}N correlation experiments and 1D dipolar-dephased ^{15}N measurements were performed on a 63 mm mid-bore 800 MHz magnet equipped with a Bruker Avance NMR console. An NHMFL 3.2 mm low-E triple-resonance biosolids MAS probe[70] was used with a ^{1}H-^{15}N double-resonance configuration optimized for ^{15}N observation. The sample spinning rate was controlled by a Bruker pneumatic MAS unit at 13 kHz ± 3 Hz. In the 2D ^{15}N-^{15}N correlation experiments, the ^{15}N magnetization was enhanced by LGCP with a contact time of 3 ms, during which the ^{1}Hs were spin-locked along the magic angle by the LG sequence and the ^{15}N B_1 field was ramped from 38.0 to 54.0 kHz[72]. The ^{15}N 90° pulse length was 5.0 μs. A SPINAL64 decoupling sequence[69] with a ^{1}H B_1 field of 83.3 kHz was used during the t_1 and t_2 dimensions. TPPI was used for quadrature detection in the t_1 dimension[73]. No ^{1}H irradiation was applied during the mixing time t_m=50 ms. The acquisition times for the t_1 and t_2 dimensions were 2.4 and 10.3 ms, respectively. In the 2D ^{1}H-^{15}N HETCOR experiments, the ^{1}H homo-nuclear decoupling was achieved using the phase-ramped frequency-switched LG sequence[75] in the t_1 dimension with an 83.3 kHz B_1 field, corresponding to 102.0 kHz decoupling amplitude along the magic angle. A short contact time of 200 μs was used to transfer ^{1}H magnetization to ^{15}N for detection under the SPINAL64 decoupling[69] with a ^{1}H B_1 field of 83 kHz. During the short contact time, the ^{1}H magnetization was spin-locked along the magic angle to further minimize long-range ^{1}H->^{15}N transfers. STATES was used for quadrature detection in the t_1 dimension[73]. For the 1D dipolar-dephased ^{15}N measurements as diagramed in the literature[65], the experimental parameters used were as follows: ^{1}H 90° pulse length of 3.0 μs,

^{15}N 180° pulse length of 10.0 μs, and a total dephasing time of four rotor periods (i.e. 307.3 μs) was used in the REDOR-based dipolar dephasing before the LG spin-lock (LGSL); during the LGSL, a ^{1}H B_1 field of 53.2 kHz was applied at an offset of +37.6 kHz resulting in the effective spin-locking field of 65.2 kHz along the magic angle. After a given LGSL time t_{SL}, a short contact time of 200 μs was used to transfer the ^{1}H magnetization to its near-by ^{15}N site for monitoring by ramping the ^{15}N B_1 field from 38.0 to 54.0 kHz. The ^{15}N signals were then acquired under the SPINAL64 decoupling[69] with a ^{1}H B_1 field of 83 kHz. The number of scans used to accumulate the signals was 20,480 with a recycle delay of 1s.

For both 600 and 800 MHz probes, the temperature calibrations were performed in separate experiments by observing ^{207}Pb chemical shift in a dilute lead nitrate (~50%) sample at their respective spinning rates, and all experiments were carried out at the calibrated temperature of −10°C. The ^{13}C chemical shifts were referenced to the carbonyl carbon resonance of glycine at 178.4 ppm relative to TMS, while the ^{15}N chemical shifts were referenced to 34.1 ppm of the glycine ammonium peak, relative to TMS based on the known relative frequency ratio between TMS (^{1}H) and liquid ammonia (^{15}N).

3. RESULTS AND DISCUSSIONS

^{13}C-^{13}C chemical shift correlation spectra

Figure 2 shows the aromatic/aromatic region of the 2D ^{13}C-^{13}C correlation spectra of the His37-labeled M2FL protein (pH 5.8) in DOPC/DOPE lipid bilayers with a mixing time of 20 ms. Since the ^{13}C-^{13}C spin diffusion is relatively efficient when mediated by abundant protons (such as PDSD[68], DARR[17], and PARIS[19]), the connectivity for all carbons in close vicinity may be established with a short mixing time (e.g. 20 ms). However, when the protons are decoupled, the proton mediation is effectively cut off such that the spin diffusion from one carbon to others become insufficient, unless a rotational resonance condition is fulfilled[76]. As documented in the SI (Figure S1), the cross peak intensities from Cβ to other carbons in the ^{13}C-labeled Fmoc-valine sample were less than 1% of the diagonal peak when SPINAL64 was applied during the mixing time, while when both PARIS and PDSD were used in the mixing time, the cross peak intensities were much stronger. For the M2FL protein at pH5.8, the ^{13}C-^{13}C correlation spectrum (with PARIS irradiation) clearly shows the cross peaks between the neutral His37 (τ) and charged His37(+) residues, i.e. Cγ/ε1(τ)-Cγ/ε1(+) as indicated in Figure 2A. These assignments were adopted from our previous work[60], where the full ^{13}C-^{13}C correlation spectrum at pH 5.8 was shown. As the four His37 residues are tightly packed at the heart of the proton conducting channel, whether these cross peaks are solely from the dipolar coupling based spin diffusion or they have also some contributions from the kinetic processes between the His37 residues is yet to be answered.

Figure 2B shows the ^{13}C-^{13}C correlation spectrum with the SPINAL64 decoupling during the mixing time. Obviously, the cross peaks between Cγ/ε1(τ) and Cδ2(τ) from the intra-His37(τ) residues disappear in the spectrum (circled regions), implying that the dipolar coupling induced spin diffusion is sufficiently suppressed. Since the inter-residue ^{13}C-^{13}C distances are longer than the intra-residue ^{13}C-^{13}C distances, it is expected that the dipolar coupling induced inter-residue ^{13}C-^{13}C spin diffusion will also be completely suppressed. As shown in Figure 2B, the cross peaks Cγ/ε1(τ)-Cγ/ε1(+) remain, although their

intensities are weakened compared to Figure 2A. Thus, such an observation is clear evidence that the neutral His37(τ) and charged His37(+) residues are inter-changing chemically.

^{15}N-^{15}N chemical shift correlation spectrum

Since ^{15}N's gyromagnetic ratio is 2.5 times smaller than ^{13}C's, the $^{15}N5^{15}N$ dipolar interaction is approximately 6.25 times less compared to a ^{13}C-^{13}C pair at the same distance. In addition, ^{15}N-^{15}N distances are greater than many ^{13}C-^{13}C distances in protein structures and hence spin diffusion resonances are rarely observable[77]. However, the molecular dynamic processes are not affected by a given spin type and therefore it is relatively easy to observe the chemical exchange processes through ^{15}N-^{15}N correlation spectra. Figure 3 shows the 2D ^{15}N-^{15}N correlation spectra of the His37-labeled M2FL protein in DOPC/DOPE lipid bilayers at pH 5.8 using a mixing time of 50 ms. Two cross peaks between the protonated nitrogens at ~166 ppm and the non-protonated nitrogens at 248.8 and 242.0 ppm are observed. As in a control experiment documented in the SI (Figure S2), no intra-histidine ^{15}N cross peaks could be observed for both the neutral τ and charged histidine in the ^{15}N-^{15}N correlation spectrum with a mixing time of 50 ms, even without ^{1}H irradiation during the mixing time. In other words, there is no observable dipolar coupling induced ^{15}N-^{15}N spin diffusion cross peak within the histidine sidechain in a 50 ms mixing time experiment. Therefore, the observed cross peaks in Figure 3 originate from inter-residue slow exchange between the neutral His37(τ) non-protonated nitrogen and charged His37(+) protonated nitrogen sites.

1D ^{15}N spin-echo spectra

It is worth noting from the diagonal signals in Fig. 3 that the protonated ^{15}N signals are dispersed from 160 ppm up to ~ 200 ppm, while the non-protonated ^{15}N signals range from 250 ppm down to 235 ppm, which suggest that either the protonated and non-protonated nitrogen sites are in the process of motional coalescing (exchange), or the various imidazole-imidazolium hydrogen bonds may be present between the neutral His37(τ) and charged His37(+) residues giving rise to a range of frequencies. Shown in the 1D spectra of Figure 4, there are two distinct ^{15}N spectral features in both the non-protontated and protonated ^{15}N region. The signals at 249.0 and 166.0 ppm are relatively narrow, while the others appear to be broad or represented by a band of frequencies. For the non-protonated ^{15}N resonances centered at 242 ppm, the signals extend to higher field (lower ppm) as low as 232 ppm. The protonated ^{15}N signals at ~174.5 spread towards lower field (higher ppm) up to 200 ppm. Such a phenomenon is typically observed when the two resonances experience a motional averaging at a rate comparable to their isotropic chemical shift difference. The ^{15}N signals observed here in Figure 4 appear to decay uniformly when the echo time was increased from 318 μs to 2.45 ms. In order to determine whether the broadening is inhomogeneous as a result of a distribution of chemically different neutral and charged His37 conformations, or homogeneous broadening due to the dynamic exchange at a rate comparable to the protonated and non-protonated ^{15}N chemical shift difference, we measured ^{15}N transverse relaxation time T_2 in the ^{15}N spin-echo spectra using a series of echo times. Figure S3 shows the ^{15}N spin-echo spectra at various echo times. The signal intensities at various chemical shift positions across the spectral range were monitored as a function of the echo times. By fitting the decay of these intensities mono-exponentially, we could obtain the T_2 values at

these specific chemical shift positions. For the signals at ~ 249 and ~166 ppm (positions a and e), the measured T_2 values are 15.7 and 12.6 ms, respectively, longer than (at least comparable to) that for the backbone amide nitrogen (position f, 11.7 ms), which do not have a large degree of motion. While the signals at ~ 240, 185, and 175 ppm (positions b, c, and d) have T_2 values of 7.1, 7.1, and 8.2 ms, respectively. The shortest T_2 value of 7.1 ms translates to a natural linewidth $\Delta\nu$ of ~45 Hz according to this equation $\Delta\nu=1/\pi T_2$, corresponding to 0.74 ppm line-broadening at an ^{15}N frequency of 60 MHz. This natural line-width is much narrower than what appears in the spectra, clearly demonstrating that the broadening is inhomogeneous, meaning that there is a distribution of chemically distinguishable neutral and charged His37 conformations, rather than the motional induced broadening at a rate comparable to the protonated and non-protonated ^{15}N chemical shift difference.

^{1}H-^{15}N HETCOR

Figure 5 shows the 2D ^{1}H-^{15}N HETCOR spectrum of the His37-labeled M2FL (pH 5.8) in DOPC/DOPE liposomes. The natural linewidth characterization by T_2 measurements are confirmed by a few well resolved resonances in this HETCOR spectrum supporting the heterogeneous broadening of the resonances and confirming that in these (pH 5.8 and 6.2) preparations the broad band of resonance intensity is not due to exchange broadening. It is evident from the spectrum that the protonated nitrogen frequencies in the His37 residues correlate with water proton frequencies. Such cross peaks between the water resonances and protons in proteins/peptides in ^{1}H-^{15}N HETCOR spectra have been observed previously[61, 63, 78–81]. In particular, Figure 5 clearly shows a few well resolved resonances with exceptionally high ^{1}H frequencies (up to 19 ppm) and high protonated ^{15}N frequencies (up to 190 ppm). Such high ^{15}N and ^{1}H frequencies strongly support the formation of short imidazole-imidazolium hydrogen bonds[64]. The linear correlation between the high ^{1}H and ^{15}N frequencies reflect multiple hydrogen-bonded states between imidazolium and imidazole with a range of distances or geometry. It is noteworthy that the resonances at ~ 13 ppm as observed in the M2FL at pH 6.2[60] that are believed to reflect the NH protons hydrogen bonded to water do not appear here in Figure 5. This suggests that the lifetime of these states is significantly shorter at pH 5.8 compared to pH 6.2.

Recovery of dipolar-dephased ^{15}N signals

In order to investigate how hydronium ions are interacting with the protons in the NH bonds of the His37 residues, we performed the newly proposed experiments[65] that probe the specific water-protein chemical exchange by spin-locking the ^{1}H magnetization along the magic angle and monitoring the recovery trajectory of dipolar-dephased ^{15}N signals. As shown in Figure 6, the ^{15}N spectra without ^{15}N dephasing (black) show similar line-shapes and intensities at different ^{1}H LGSL time, t_{SL}. As a short contact time (i.e. 200 μs) was used to transfer the ^{1}H magnetization to ^{15}N, only the ^{15}N signals from the protonated ^{15}N sites of His37 sidechains were cross-polarized (i.e. the $\boldsymbol{\tau}$ state N$\boldsymbol{\varepsilon 2\tau}$ and the charged states N$\delta 1^{+}$ and N$\varepsilon 2^{+}$) resulting in the non-protonated $\boldsymbol{\tau}$ state N$\boldsymbol{\delta 1\tau}$ (at ~ 250 ppm) being hardly polarized. Again, the observed ^{15}N resonances are spread from 165 to ~200 ppm. When the ^{15}N selective dephasing was applied, the protons of the N$\boldsymbol{\varepsilon 2\tau}$ sites and the charged His37 H5N$\delta 1^{+}$ and H-N$\varepsilon 2^{+}$ sites were dephased at the beginning of the LGSL and hence no ^{15}N

signals from these protonated sites would be expected. However, in the presence of the water-protein exchange, the protons from the τ state Nε2τ and the charged His37 H-Nδ1$^+$ or H-Nε2$^+$ (presumably H-Nε2$^+$) could be re-polarized during the LGCP, such that the signals from these protonated sites could be observed at a short t_{SL}. As shown in the red spectra of Figure 6, the observed ^{15}N signals were largely reduced at a short t_{SL} of 50 μs, especially the signals at ~166 ppm. As t_{SL} increased, the dipolar-dephased ^{15}N signals from the protonated ^{15}N sites gained more intensity, implying that their bonded protons gain magnetization during the LGSL. As ^{1}H spin diffusion is suppressed during the LGSL and any relayed transfer is largely eliminated, the observed gain can only be facilitated by chemical exchange between this particular proton and the hydronium ions.

A series of 1D dipolar-dephased ^{15}N signals as a function of t_{SL} would permit the monitoring of chemical exchange processes between the hydronium ions and the protons in the His37 NH bonds. The recovery trajectory of these dipolar-dephased ^{15}N signal intensities can be fitted[65] using the following equation to obtain their exchange rate constant k_{IM}:

$$I\left(t_{SL}\right)=I(0)+pM\left(0\right)\left\{1-\exp[-(p+1)k_{IM}t_{SL})]\right\}\exp\left(-t_{SL}/T_{1\rho}^{H}\right)/(p+1). \quad [1]$$

Here p is the hydronium ion concentration in the pool of water molecules, $T_{1\rho}^{H}$ is the spin-lattice relaxation time in the LGSL field for protons in water molecules and in the His37 NH bonds (with the assumption that they have the same spin-lattice relaxation time in the LGSL field), and $I(0)$ represents an initial ^{15}N signal intensity. This initial term $I(0)$ should include a contribution from any incomplete HN dephasing by REDOR due to various NH bond lengths and re-polarized signals during the LGCP period according to the exchange rate constant and the LGCP contact time.

Figure 7 shows the plot of the dipolar-dephased ^{15}N signals versus t_{SL}. In order to reduce the number of the fitting variables, we measured $T_{1\rho}^{H}$ in separate experiments, yielding $T_{1\rho}^{H}$ = 15.8 ms (Figure S4). We used this value as a constant to fit the recovery trajectory using Equation 1 to obtain $(1+p)k_{IM}$=4,000 ± 1,500 s^{-1}. The concentration p of the hydronium ions in the M2 channel pore is about 10^{-6} M with the assumption that the pH in the pore is the same as in the bulk environment. Thus, the exchange rate constant between hydronium ions and the protons in the His37 NH bonds for the M2FL is on the order of 4,000 ± 1,500 s^{-1} for pH 5.8 at −10°C, which is about twice as fast as for the M2FL for pH 6.2[65], indicating that the increase of the proton dynamics at lower pH is directly proportional to the proton concentration. Again, this represents an average value over a number of different His37 states with various exposures to hydronium ions. It is anticipated that the exchange model[60, 65] established at −10° should be relevant at the physiological temperature but the exchange rates should be faster.

Conductance mechanism

Despite the chemical complexity of the His37 states, a model for how the hydronium ions go through the His37 tetrad in the M2 proton channel has been established[65]. Here we use this

model to interpret our experimental results in detail. The “initial” NH protons in the His tetrad are colored green and blue for the imidazole-imidazolium hydrogen-bonded His C-D pair, respectively, as shown in the upper left panel of Figure 8. The hydronium ion based proton is colored red. When the hydronium ion is attracted by the non-protonated N$\delta 1\tau$ site, the neutral His37 residue D becomes charged, so that both C and D residues are charged, consequently breaking the imidazole-imidazolium H-bond (upper right in Figure 8). The two imidazolium residues conformationally rearrange, due to steric clash and charge repulsion with the newly protonated N$\delta 1^{+}$H (D) site oriented toward the pool of externally exposed waters, while the original N$\varepsilon 2^{+}$H (C) and the newly formed N$\varepsilon 2^{+}$H (D) are both exposed to waters of the viral interior, as illustrated in Figure 9. The return of the His N$\delta 1^{+}$H (D) proton to the waters of the viral exterior (path I) results in a futile cycle, as illustrated by the red arrow and red circle in Figure 9, however, both His N$\varepsilon 2^{+}$H (C and D) protons are accessible by interior waters. The absorbance of either His N$\varepsilon 2^{+}$H proton by waters of the viral interior (green (II) and blue (III) arrows) result in successful conductance of a proton across the membrane. If the His N$\varepsilon 2^{+}$H (C) proton (the original imidazole-imidazolium H-bonded proton) is reabsorbed by water (path II in Figure 8), the imidazolium donates its H-N$\delta 1$ (D) proton to reform the same His37 C-D pair with an imidazolium-imidazole hydrogen-bond utilizing a π state. This proton rapidly rearranges crossing the H-bond barrier to form a more stable τ-charge H-bonded pair, as in the original state and as illustrated in the lower right panel of Figure 8. When an interior water reabsorbs the proton of the newly formed N$\varepsilon 2^{+}$H (D), D becomes a π state and forms a new imidazolium-imidazole H-bond with H-N$\delta 1$ of His A (path III in Figure 8) with the proton rapidly crossing the H-bond barrier to form a τ-charge hydrogen bonded pair, leading to a rotation of the imidazolium-imidazole bonding pairs[51], as shown in the lower left panel of Figure 8. Consequently the imidazolium-imidazole bonding pairs are reestablished and ready to accept next hydronium ion. This process for His37 τ-states accepting protons from hydronium ions is essential for the buildup of the dipolar-dephased ^{15}N signals as a function of t_{SL}.

It has been clear for decades that the proton conductance in the M2 channel was facilitated by the His37 residues, but the question has been how the His37 tetrad facilitates this process. With the imidazolium-imidazole bonding His-His pairs, the LBHB model was established, i.e. the proton is transferred through the breaking and reforming of the H-bonds between the two pairs of His37 dimers facilitated by hydronium attack[36, 51, 60]. If the His37 does not form imidazole-imidazolium hydrogen bonds, but only directly hydrogen bonds with water, the proton shuttling mechanism is proposed, in which individual His37 residues shuttles protons by imidazole ring reorientations and proton exchange with water without the process of forming any inter-monomer hydrogen bond between the His37 residues[61, 63]. Our experimental data presented here strongly supports the LBHB mechanism, as explained in the following.

First, the observation of high ^{1}H frequencies (up to 19 ppm) and high ^{15}N frequencies (up to 190 ppm) in the ^{1}H-^{15}N HETCOR spectrum (Figure 5) indicates the existence of the imidazolium-imidazole bonds between His-His pairs. The long T_2 values (> 7 ms) for the ^{15}N resonances at ~240, ~185, and 175 ppm confirm that the broadening is inhomogeneous in nature corresponding to a distribution of chemically distinct His37 conformational states, rather than the exchange-induced homogeneous broadening.

Secondly, it is evident from the ^{1}H-^{15}N HETCOR spectrum in Figure 5 that the ^{15}N resonances at ~ 166 ppm are weakly correlated with water molecules as compared to the signals at ~ 175 ppm. In the dipolar-dephased ^{15}N spectra in Figure 6, the dephased ^{15}N signals at ~175 ppm almost recovered to their full intensities with a LGSL time of 2000 μs, while only a fraction of the signals at ~166 ppm regained their intensity. This suggests that the ^{15}N sites resonating at ~166 ppm are discriminately less accessible by water. However, it is these signals at ~166 ppm that correlate with the non-protonated nitrogen sites at ~248 ppm in the ^{15}N-^{15}N EXSY spectrum (e.g. Figure 3). These observations are hard to explain with the proton shuttling mechanism, in which all ^{15}N sites in either neutral or charged states should have equal accessibility by water, but in the LBHB mechanism unequal accessibility is easy to explain. As illustrated in path III in Figure 8, the hydronium ion from the exterior water goes to the N$\delta1^{+}$H (D), while the initial (i.e. before the breaking of the imidazole-imidazolium hydrogen bond as in the upper left of Figure 8) His37 (D) was a neutral state N$\delta1\tau$ (D). Therefore, the ^{15}N-^{15}N exchange observed here, in fact, represents the dynamic process between the neutral and charged states in the same His37 residue. This argument is also supported by the ^{13}C-^{13}C EXSY spectrum in Figure 2B, showing the chemical exchanged resonances between the neutral and charged His37 residues. While in the path II of Figure 8, the proton in the N$\delta1^{+}$H (C) is virtually not accessible at all by the hydronium ions. As the non-protonated and protonated ^{15}N signals are well separated, it may be possible to characterize the dynamic process taking place only in path III by using 1D ^{15}N pure exchange spectroscopy[82, 83], although the sensitivity is intrinsically low.

Thirdly, the recovery of the dipolar-dephased ^{15}N signals as a function of LGSL time, as observed here, further discriminates the proton shuttling mechanism[61, 63] in the M2FL proton channel in lipid bilayers. In our dipolar-dephased ^{15}N measurements, all protonated ^{15}N signals are initially minimized and should remain minimal during the LGSL except for those NH bonds whose protons are exchangeable with hydronium ions. As in the proton shuttling mechanism[61, 63], the non-protonated ^{15}N site by accepting a proton from a hydronium ion originating from the viral exterior becomes protonated and thus is not capable of receiving next hydronium ion as it has to remain facing the viral exterior so that the other ^{15}N site in the same His residue can be ready to release its proton to the viral interior. Furthermore, this proton transport seems to involve only the protonation and de-protonation of the neutral His37 residues. In other words, the protonated ^{15}N signals from the charged His37 residues should not regain any intensity when dephased, but the protonated ^{15}N signals from the neutral His37 residues are expected to recover fully. This is contradictory with our experimental data shown in Figures 6 and 7, where the protonated ^{15}N signals at ~175 ppm from the charged His37 sites almost recover to their full intensities and only a fraction of the signals at ~166 ppm (partly from the neutral His37 residues) have regained their intensity. On the other hand, these experimental observations can be well explained by the LBHB model: 1) the reformed imidazole-imidazolium hydrogen bonding His37 pairs always allow the His37 tetrad to be ready for accepting next hydronium ion. 2) In the His37 tetrad, as illustrated in Figure 8, all the circled protons are dephased in applying the ^{15}N REDOR dephasing sequence. But those in bold and color highlighted protons would regain their intensities as the hydronium ions are taking their positions through the exchange processes, including both protonated ^{15}N sites from the neutral *and* charged His37 residues.

It is worth noting that in path II shown in Figure 8, only the protons in the imidazole-imidazolium H-bonds are in exchange with the hydronium ions. It could be understood as follows: due to the oligomeric helix packing effect, the reformed imidazole-imidazolium hydrogen bond in the lower right panel in Figure 8 may not have the same hydrogen bonding geometry as in the initial imidazole-imidazolium hydrogen bond in the upper left panel, leading to a distribution of hydrogen bonds with different strengths, thus chemically distinct resonances in the ^{1}H-^{15}N HETCOR spectrum in Figure 5. This is supported by the presence of the slightly off-diagonal peaks of the protonated ^{15}N signals in the ^{15}N-^{15}N correlation spectrum in Figure 3. This heterogeneity in imidazole-imidazolium resonance frequencies is also supported by several large hydrophobic residues in the helix-helix interface that could generate through various rotameric states slightly difference imidazole-imidazolium geometries resulting in the variety of observed resonance frequencies.

4. CONCLUSION

Unique functional insights associated with the His37 tetrad, the heart of proton conductance in the M2 proton channel, have been achieved by solid-state NMR experiments. It is confirmed through the existence of chemical exchange spectroscopy between the neutral and charged His37 residues using both ^{13}C-^{13}C and ^{15}N-^{15}N EXSY spectra that the exchange may involve an inter-conversion between the neutral and charged conformations of the His37 residues. Although broad protonated and non-protonated ^{15}N resonance bands were observed, they have relatively long T_2 values, requiring that the band of resonances is inhomogeneous in nature, rather than exchange-induced, thus confirming the presence of chemically distinct conformational states of the His37 residues. Our experimental results provide conclusive evidence for the formation of imidazolium-imidazole hydrogen bonds in the histidine tetrad at low pH values and thus support the LBHB model for the proton conductance mechanism in the full length M2 protein. The recovery trajectory of the dipolar-dephased ^{15}N signals allows us to determine the exchange rate constant of ~4000 s^{-1} at pH 5.8 and −10°C between the hydronium ions and the protons in the His37 NH bonds at the heart of the M2 proton conduction mechanism. From a functional biology point of view, unique solid-state NMR experiments, as featured herein can be used to characterize detailed structure-function relationships of membrane-bound species at the water-protein interface, and in particular to understand the rates for hydrogen bond formation and breaking in biological systems during proton transport, such as in the M2 proton channel.

Supplementary Material

Refer to Web version on PubMed Central for supplementary material.

Acknowledgments

This work was supported by NIH Grant AI23007 and AI119178. All NMR experiments were carried out at the National High Magnetic Field Lab (NHMFL) supported by the NSF Cooperative agreement N. DMR-1157490 and the State of Florida.

ABBREVIATIONS

MAS	magic angle spinning
TM	transmembrane
M2FL	full length M2
DOPC	1,2-dioleoyl-*sn*-glycero-3-phosphocholine
DOPE	1,2-dioleoyl-*sn*-glycero-3-phosphoethanolamine
POPC	1-palmitoyl-2-oleoyl-sn-glycero-3-phosphatidylcholine
E. coli	Escherichia coli
DPhPC	1,2-diphytanoyl-sn-glycero-3-phosphocholine
H-bond	hydrogen-bond
PARIS	phase-alternated recoupling irradiation scheme
DARR	dipolar assisted rotational resonance
SPINAL	small phase incremental alternation
HETCOR	heteronuclear correlation
LBHB	low-barrier hydrogen bond
1D	one-dimensional
2D	two-dimensional
EXSY	exchange spectroscopy
PDSD	proton-driven spin diffusion
CP	cross polarization
LG	Lee-Goldburg
LGCP	Lee-Goldburg cross polarization
LGSL	Lee-Goldburg spin lock
REDOR	rotational-echo double-resonance

References

1. McMahon HT, Gallop JL. Membrane Curvature Mechanisms of Dynamic Cell Membrane Remodelling. Nature. 2005; 438:590–596. [PubMed: 16319878]
2. Groves JT, Kuriyan J. Molecular Mechanisms in Signal Transduction at the Membrane. Nat Struct Mol Biol. 2010; 17:659–665. [PubMed: 20495561]
3. Schmick M, Bastiaens PIH. The Interdependence of Membrane Shape Cellular Signal Processing. Cell. 2014; 156:1132–1138. [PubMed: 24630717]

4. Cross TA, Sharma M, Yi M, Zhou HX. Influence of Solubilizing Environments on Membrane Protein Structures. Trends Biochem Sci. 2011; 36:117–125. [PubMed: 20724162]
5. Duerr UHN, Gildenberg M, Ramamoorthy A. The Magic of Bicelles Lights up Membrane Protein Structure. Chem Rev. 2012; 112:6054–6074. [PubMed: 22920148]
6. Miao Y, Cross TA. Solid State NMR Protein-Protein Interactions in Membranes. Curr Opin Struct Biol. 2013; 23:919–928. [PubMed: 24034903]
7. Huster D. Solid-state Nmr Spectroscopy to Study Protein-Lipid Interactions. Biochim Biophys Acta. 2014; 1841:1146–1160. [PubMed: 24333800]
8. Krepkiy D, Gawrisch K, Swartz KJ. Structural Interactions between Lipids Water and S1-S4 Voltage-Sensing Domains. J Mol Biol. 2012; 423:632–647. [PubMed: 22858867]
9. Saito H, Ando I, Ramamoorthy A. Chemical Shift Tensor—the Heart of NMR: Insights into Biological Aspects of Proteins. Prog Nucl Magn Reson Spectrosc. 2010; 57:181–228. [PubMed: 20633363]
10. Eilers M, Patel AB, Liu W, Smith SO. Comparison of Helix Interactions in Membrane Soluble α-Bundle Proteins. Biophys J. 2002; 82:2720–2736. [PubMed: 11964258]
11. Walian P, Cross TA, Jap BK. Structural Genomics of Membrane Proteins. Genome Biology. 2004; 5:215. [PubMed: 15059248]
12. Soubias O, Gawrisch K. The Role of the Lipid Matrix for Structure Function of the Gpcr Rhodopsin. Biochim Biophys Acta. 2012; 1818:234–240. [PubMed: 21924236]
13. Zhou HX, Cross TA. Influences of Membrane Mimetic Environments on Membrane Protein Structures. Annu Rev Biophys. 2013; 42:361–392. [PubMed: 23451886]
14. Wuthrich, K. NMR of Proteins and Nucleic Acids. Wiley; New York, NY: 1986.
15. Straus SK, Bremi T, Ernst RR. Experiments Strategies for the Assignment of Fully $^{13}C/^{15}N$-Labelled Polypeptides by Solid State Nmr. J Biomol NMR. 1998; 12:39–50. [PubMed: 9729787]
16. Bloembergen N. On the Interaction of Nuclear Spins in a Crystalline Lattice. Physica. 15:386–426. 15.
17. Takegoshi K, Nakamura S, Terao T. C-13-H-1 Dipolar-Assisted Rotational Resonance in Magic-Angle Spinning Nmr. Chem Phys Lett. 2001; 344:631–637.
18. Hou G, Yan S, Sun S, Han Y, Byeon IL, Ahn J, Concel J, Samosom A, Gronenborn AM, Polenova T. Spin Diffusion Driven by R-Symmetry Sequences: Applications to Homonuclear Correlation Spectroscopy in Mas Nmr of Biological Organic Solids. J Am Chem Soc. 2011; 133:3943–3953. [PubMed: 21361320]
19. Weingarth M, Demco DE, Bodenhausen G, Tekely P. Improved Magnetization Transfer in Solid-State NMR with Fast Magic Angle Spinning. Chem Phys Lett. 2009; 469:342–348.
20. Wei YF, Ramamoorthy A. 2D ^{15}N-^{15}N Isotropic Chemical Shift Correlation Established by ^{1}H-^{1}H Dipolar Coherence Transfer in Biological Solids. Chem Phys Lett. 2001; 342:312–316.
21. Lewandowski JR, De Paepe G, Eddy MT, Struppe JO, Maas W, Griffin RG. Proton Assisted Recoupling at High Spinning Frequencies. J Phys Chem B. 2009; 113:9062–9069. [PubMed: 19489532]
22. Straaso LA, Shankar R, Tan KO, Hellwagner J, Meier BH, Hansen MR, Nielsen NC, Vosegaard T, Ernst M, Nielsen AB. Improved Transfer Efficiencies in Radio-Frequency-Driven Recoupling Solid-State Nmr by Adiabatic Sweep through the Dipolar Recoupling Condition. J Chem Phys. 2016; 145:034201. [PubMed: 27448878]
23. Jaroniec CP, Filip C, Griffin RG. 3D TEDOR NMR Experiments for Simultaneous Measurement of Multiple Carbon-Nitrogen Distances in Umiformly ^{13}C ^{15}N-Labeled Solids. J Am Chem Soc. 2002; 124:10728–10742. [PubMed: 12207528]
24. Hong M. Resonance Assignment of C-13/N-15 Labeled Solid Proteins by Two and Three-Dimensional Magic-Angle-Spinning Nmr. J Biomol NMR. 1999; 15:1–14. [PubMed: 10549131]
25. Baldus M, Petkova AT, Herzfeld J, Griffin RG. Cross Polarization in the Tilted Frame: Assignment Spectral Simplification in Heteronuclear Spin Systems. Mol Phys. 1998; 95:1197–1207.
26. Rienstra CM, Hohwy M, Hong M, Griffin RG. 2D 3D N-15–C-13–C-13 NMR Chemical Shift Correlation Spectroscopy of Solids: Assignment of MAS Spectra of Peptides. J Am Chem Soc. 2000; 122:10979–10990.

27. Pauli J, Baldus M, van Rossum B, de Groot H, Oschkinat H. Backbone Side-Chain C-13 N-15 Signal Assignments of the Alpha-Spectrin SH3 Domain by Magic Angle Spinning Solid-state NMR at 17.6 Tesla. Chem Biochem. 2001; 2:272–281.
28. Miao Y, Cross TA, Fu R. Identifying Inter-residue Resonances in Crowded 2D ^{13}C-^{13}C Chemical Shift Correlation Spectra of Membrane Proteins by Solid-state Mas NMR Difference Spectroscopy. J Biomol NMR. 2013; 56:265–273. [PubMed: 23708936]
29. Wang T, William JK, Schmidt-Rohr K, Hong M. Relaxation-Compensated Difference Spin Diffusion NMR for Detecting ^{13}C-^{13}C Long-range Correlations in Proteins Polysaccharides. J Biomol NMR. 2015; 61:97–107. [PubMed: 25510834]
30. Sugrue RJ, Hay AJ. Structural Characteristics of the M2 Protein of Influenza-A Viruses - Evidence That It Forms a Tetrameric Channel. Virology. 1991; 180:617–624. [PubMed: 1989386]
31. Sakaguchi T, Tu QA, Pinto LH, Lamb RA. The Active Oligomeric State of the Minimalistic Influenza Virus M-2 Ion Channel Is a Tetramer. Proc Natl Acad Sci USA. 1997; 94:5000–5005. [PubMed: 9144179]
32. Hu J, Asbury T, Achuthan S, Li C, Bertram R, Quine JR, Fu R, Cross TA. Backbone Structure of the Amantadine-Blocked Trans-Membrane Domain M2 Proton Channel from Influenza A Virus. Biophys J. 2007; 92:4335–4343. [PubMed: 17384070]
33. Nishimura K, Kim SG, Zhang L, Cross TA. The Closed State of a H+ Channel Helical Bundle Combining Precise Orientational Distance Restraints from Solid State Nmr. Biochemistry. 2002; 41:13170–13177. [PubMed: 12403618]
34. Lamb RA, Zebedee SL, Richardson CD. Influenza Virus-M2 Protein Is an Integral Membrane-Protein Expressed on the Infected-Cell Surface. Cell. 1985; 40:627–633. [PubMed: 3882238]
35. Grambas S, Bennett MS, Hay AJ. Influence of Amantadine Resistance Mutations on the pH Regulatory Function of the M2-Protein of Influenza-A Viruses. Virology. 1992; 191:541–549. [PubMed: 1448912]
36. Hu J, Fu R, Nishimura K, Zhang L, Zhou HX, Busath DD, Vijayvergiya V, Cross TA. Histidines Heart of the Hydrogen Ion Channel from Influenza a Virus: Toward an Understanding of Conductance Proton Selectivity. Proc Natl Acad Sci USA. 2006; 103:6865–6870. [PubMed: 16632600]
37. Schnell JR, Chou JJ. Structure Mechanism of the M2 Proton Channel of Influenza A Virus. Nature. 2008; 451:591–595. [PubMed: 18235503]
38. Tian CL, Gao PF, Pinto LH, Lamb RA, Cross TA. Initial Structural Dynamic Characterization of the M2 Protein Transmembrane Amphipathic Helices in Lipid Bilayers. Protein Sci. 2003; 12:2597–2605. [PubMed: 14573870]
39. Nguyen PA, Soto CS, Polishchuk A, Caputo GA, Tatko CD, Ma C, Ohigashi Y, Pinto LH, DeGrado WF, Howard KP. pH-Induced Conformational Change of the Influenza M2 Protein C-Terminal Domain. Biochemistry. 2008; 47:9934–9936. [PubMed: 18754675]
40. Ma C, Polishchuk AL, Ohigashi Y, Stouffer AL, Schoen A, Magavern E, Jing X, Lear JD, Freire E, Lamb RA, et al. Identification of the Functional Core of the Influenza A Virus A/M2 Proton-Selective Ion Channel. Proc Natl Acad Sci USA. 2009; 106:12283–12288. [PubMed: 19590009]
41. Rossman JS, Jing X, Leser GP, Lamb RA. Influenza Virus M2 Protein Mediates Escrt-Independent Membrane Scission. Cell. 2010; 142:902–913. [PubMed: 20850012]
42. Miao Y, Qin H, Fu R, Sharma M, Can TV, Hung I, Luca S, Gor'kov PL, Brey WW, Cross TA. M2 Proton Channel Structural Validation from Full-Length Protein Samples in Synthetic Bilayers *E. Coli* Membranes. Angew Chem. 2012; 124:8508–8511.
43. Can TV, Sharma M, Hung I, Gor'kov PL, Brey WW, Cross TA. Magic Angle Spinning Oriented Sample Solid-state NMR Structural Restraints Combine for Influenza a M2 Protein Functional Insights. J Am Chem Soc. 2012; 134:9022–9025. [PubMed: 22616841]
44. Cady SD, Schmidt-Rohr K, Wang J, Soto CS, DeGrado WF, Hong M. Structure of the Amantadine Binding Site of Influenza M2 Proton Channels in Lipid Bilayers. Nature. 2010; 463:689–692. [PubMed: 20130653]
45. Cady SD, Mishanina TV, Hong M. Structure of Amantadine-Bound M2 Transmembrane Peptide of Influenza A in Lipid Bilayers from Magic-Angle-Spinning Solid-state NMR: The Role of Ser31 in Amantadine Binding. J Mol Biol. 2009; 385:1127–1141. [PubMed: 19061899]

46. Andreas LB, Eddy MT, Pielak RM, Chou JJ, Griffin RG. Magic Angle Spinning NMR Investigation of Influenza A $M2_{18–60}$: Support for an Allosteric Mechanism of Inhibition. J Am Chem Soc. 2010; 132:10958–10960. [PubMed: 20698642]
47. Andreas LB, Eddy MT, Chou JJ, Griffin RG. Magic-Angle-Spinning NMR of the Drug Resistant S31N M2 Proton Transporter from Influenza A. J Am Chem Soc. 2012; 134:7215–7218. [PubMed: 22480220]
48. Colvin MT, Andreas LB, Chou JJ, Griffin RG. Proton Association Constants of His 37 in the Influenza-A M218-60 Dimer-of-Dimers. Biochemistry. 2014; 53:5987–5994. [PubMed: 25184631]
49. Andreas LB, Reese M, Eddy MT, Gelev V, Ni QZ, Miller EA, Emsley L, Pintacuda G, Chou JJ, Griffin RG. Structure Mechanism of the Influenza A M218-60 Dimer of Dimers. J Am Chem Soc. 2015; 137:14877–14886. [PubMed: 26218479]
50. Du J, Cross TA, Zhou HX. Recent Progress in Structure-Based Anti-Influenza Drug Design. Drug Discov Today. 2012; 17:1111–1120. [PubMed: 22704956]
51. Sharma M, Yi M, Dong H, Qin H, Peterson E, Busath DD, Zhou HX, Cross TA. Insight into the Mechanism of the Influenza a Proton Channel from a Structure in a Lipid Bilayer. Science. 2010; 330:509–512. [PubMed: 20966252]
52. Wang J, Wu Y, Ma C, Fiorin G, Wang J, Pinto LH, Lamb RA, Klein ML, Degrado WF. Structure Inhibition of the Drug-Resistant S31n Mutant of the M2 Ion Channel of Influenza a Virus. Proc Natl Acad Sci USA. 2013; 110:1315–1320. [PubMed: 23302696]
53. Wang JF, Kim SG, Kovacs F, Cross TA. Structure of the Transmembrane Region of the M2 Protein H+ Channel. Protein Sci. 2001; 10:2241–2250. [PubMed: 11604531]
54. Pielak RM, Schnell JR, Chou JJ. Mechanism of Drug Inhibition Drug Resistance of Influenza A M2 Channel. Proc Natl Acad Sci USA. 2009; 106:7379–7384. [PubMed: 19383794]
55. Pielak RM, Oxenoid K, Chou JJ. Structural Investigation of Rimantadine Inhibition of the AM2-BM2 Chimera Channel of Influenza Viruses. Structure. 2011; 19:1655–1663. [PubMed: 22078564]
56. Pielak RM, Chou JJ. Solution NMR Structure of the V27A Drug Resistant Mutant of Influenza a M2 Channel. Biochem Biophys Res Commun. 2010; 401:58–63. [PubMed: 20833142]
57. Stouffer AL, Acharya R, Salom D, Levine AS, Di Costanzo L, Soto CS, Tereshko V, Nanda V, Stayrook S, DeGrado WF. Structural Basis for the Function Inhibition of an Influenza Virus Proton Channel. Nature. 2008; 451:596–599. [PubMed: 18235504]
58. Acharya R, Carnevale V, Fiorin G, Levine BG, Polishchuk AL, Balannik V, Samish I, Lamb RA, Pinto LH, DeGrado WF, et al. Structure and Mechanism of Proton Transport through the Transmembrane Tetrameric M2 Protein Bundle of the Influenza a Virus. Proc Natl Acad Sci USA. 2010; 107:15075–15080. [PubMed: 20689043]
59. Liao SY, Yang Y, Tietze D, Hong M. The Influenza M2 Cytoplasmic Tail Changes the Proton-Exchange Equilibra the Backbone Conformation of the Transmembrane Histidine Residue to Facilitate Proton Conduction. J Am Chem Soc. 2015; 137:6067–6077. [PubMed: 25892574]
60. Miao Y, Fu R, Zhou HX, Cross TA. Dynamic Short Hydrogen Bonds in Histidine Tetrad of Full Length M2 Proton Channel Reveal Tetrameric Structural Heterogeneity Functional Mechanism. Structure. 2015; 23:2300–2308. [PubMed: 26526851]
61. Hong M, Fritzsching KJ, William JK. Hydrogen-Bonding Partner of the Proton-Conducting Histidine in the Influenza M2 Proton Channel Revealed from ^{1}H Chemical Shifts. J Am Chem Soc. 2012; 134:14753–14755. [PubMed: 22931093]
62. Witter R, Nozirov F, Stemberg U, Cross TA, Ulrich AS, Fu R. Solid-state ^{19}F NMR Spectroscopy Reveals That Trp_{41} Participates in the Gating Mechanism of the M2 Proton Channel of Influenza A Virus. J Am Chem Soc. 2008; 130:11905–11913.
63. Hu F, Schmidt-Rohr K, Hong M. NMR Detection of pH-Dependent Histidine-Water Proton Exchange Reveals the Conduction Mechanism of a Transmembrane Proton Channel. J Am Chem Soc. 2012; 134:3703–3713. [PubMed: 21974716]
64. Eckert H, Yesinowski JP, Silver LA, Stolper EM. Water in Silicate Glasses: Quantitation Structural Stidies by Proton Solid Echo Magic Angle Spinning NMR Methods. J Phys Chem. 1988; 92:2055–2064.

65. Fu R, Miao Y, Qin H, Cross TA. Probing Hydronium Ion Histidine NH Exchange Rate Constants in the M2 Channel Via Indirect Observation of Dipolar-Dephased ^{15}N Signals in Solid-state Magic-Angle-Spinning Nmr. J Am Chem Soc. 2016; 138:15801–15804. [PubMed: 27960325]
66. Ekanayake EV, Fu R, Cross TA. Structural Influences: Cholesterol Drug and Proton Binding to Full-Length Influenza a M2 Protein. Biophys J. 2016; 110:1391–1399. [PubMed: 27028648]
67. Levitt, MH. Spin Dynamics: Basics of Nuclear Magnetic Resonance. 2nd. John Wiley & Sons, Ltd; 2008.
68. Bloembergen N, Shapiro S, Pershan PS, Artman JO. Cross-Relaxation in Spin Systems. Phys Rev. 1959; 114:445–459.
69. Fung BM, Khitrin AK, Ermolaev K. An Improved Broadband Decoupling Sequence for Liquid Crystals Solids. J Magn Reson. 2000; 142:97–101. [PubMed: 10617439]
70. Gor'kov PL, Chekmenev EY, Cotten M, Buffy JJ, Traaseth NJ, Veglia G, Brey WW. Using Low-E Resonators to Reduce RF Heating in Biological Samples for Static Solid-state NMR up to 900 Mhz. J Magn Reson. 2007; 185:77–93. [PubMed: 17174130]
71. McNeill SA, Gor'kov PL, Shetty K, Brey WW, Long JR. A Low-E Magic Angle Spinning Probe for Biological Solid State NMR at 750 Mhz. J Magn Reson. 2009; 197:135–144. [PubMed: 19138870]
72. Peersen OB, Wu XL, Smith SO. Enhancement of CP-MAS Signals by Variable-Amplitude Cross-Polarization - Compensation for Inhomogeneous B-1 Fields. J Magn Reson A. 1994; 106:127–131.
73. Bodenhausen G, Vold RL, Vold RR. Multiple Quantum Spin-Echo Spectroscopy. J Magn Reson. 1980; 37:93–106.
74. Fu R, Hu J, Cross TA. Towards Quantitative Measurements in Solid-state CPMAS NMR: A Lee-Goldburg Frequency Modulated Cross-Polarization Scheme. J Magn Reson. 2004; 168:8–17. [PubMed: 15082244]
75. Bielecki A, Kolbert AC, De Groot H, Griffin RG, Levitt MH. Frequency-Switched Lee-Goldburg Sequences in Solids. Adv Magn Reson. 1990; 14:111–150.
76. Colombo MG, Meier BH, Ernst RR. Rotor-Driven Spin Diffusion in Natural-Abundance ^{13}C Spin Systems. Chem Phys Lett. 1988; 146:189–196.
77. Cross TA, Frey MH, Opella SJ. ^{15}N Spin Exchange in a Protein. J Am Chem Soc. 1983; 105:7471–7473.
78. Fu R, Gordon ED, Hibbard DJ, Cotten M. High Resolution Heteronuclear Correlation NMR Spectroscopy of an Anitimicrobial Peptide in Aligned Lipid Bilayers: Peptide-Water Interactions at the Water-Bilayer Interface. J Am Chem Soc. 2009; 131:10830–10831. [PubMed: 19621928]
79. Lesage A, Emsley L, Penin F, Bockmann A. Investigation of Dipolar-Mediated Water-Protein Interactions in Microcrystalline Crh by Solid-state NMR Spectroscopy. J Am Chem Soc. 2006; 128:8246–8255. [PubMed: 16787089]
80. Harbison GS, Roberts JE, Herzfeld J, Griffin RG. Solid-state NMR Detection of Proton Exchange between the Bacteriorhodopsin Schiff Base Bulk Water. J Am Chem Soc. 1988; 110:7221–7223.
81. Bockmann A, Juy M, Bettler E, Emsley L, Galinier A, Penin F, Lesage A. Water-Protein Hydrogen Exchange in the Micro-Crystalline Protein Crh as Observed by Solid State NMR Spectroscopy. J Biomol NMR. 2005; 32:195–207. [PubMed: 16132820]
82. deAzevedo ER, Bonagamba TJ, Schmidt-Rohr K. Pure-Exchange Solid-state NMR. J Magn Reson. 2000; 142:86–96. [PubMed: 10617438]
83. Cho MK, Gayen A, Banigan JR, Leninger M, Traaseth NJ. Intrinsic Conformational Plasticity of Native Emre Provides a Pathway for Multidrug Resistance. J Am Chem Soc. 2014; 136:8072–8080. [PubMed: 24856154]

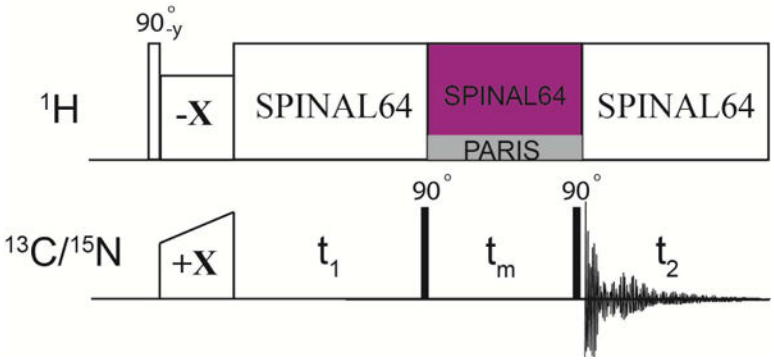

Figure 1.

Pulse sequence used for homonuclear correlation experiments. During the mixing time t_m, three different irradiation methods are applied: PARIS (grey), no irradiation (i.e. PDSD), and SPINAL64 (purple).

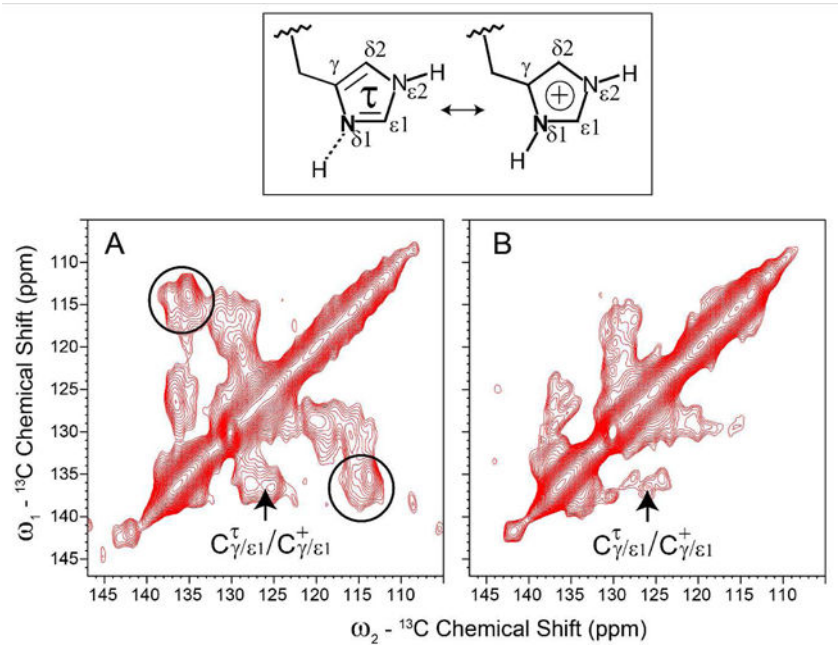

Figure 2.

(Top) Schematics for the τ and charged histidine sidechains. (Bottom) Aromatic/aromatic region of 2D ^{13}C-^{13}C correlation spectra of the His37-labeled M2FL (pH 5.8) in DOPC/DOPE liposomes with a mixing time of 20ms, during which the PARIS (A) and SPINAL64 (B) irradiation were applied on the ^{1}H channel. The circled regions indicate the cross peaks between Cγ/ε1(τ) and Cδ2(τ) from the His37(τ) residues.

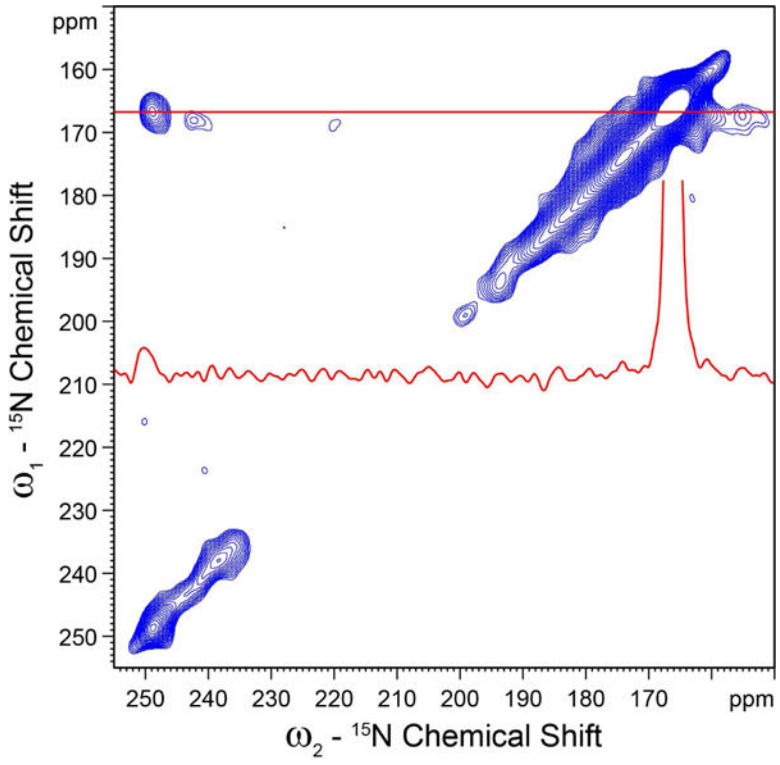

Fig. 3.

2D ^{15}N-^{15}Ncorrelation (EXSY) spectrum of the His37-labeled M2FL (pH 5.8) in DOPC/DOPE liposomes. No 1H irradiation was applied on the ^{1}H channel during a mixing time of 50 ms. The red 1D spectrum was taken from the 2D spectrum along the red line at 166.3 ppm.

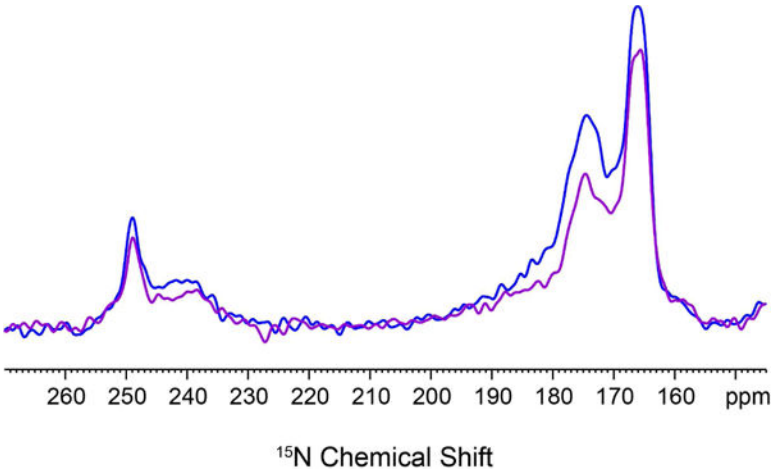

Figure 4.

Aromatic region of 1D ^{15}N spin-echo spectra of the His37-labeled M2FL (pH 5.8). A total of 4 (Blue) and 15 (Purple) rotor periods were used for the spin echo times, corresponding to 318 μs and 2.45 ms, respectively.

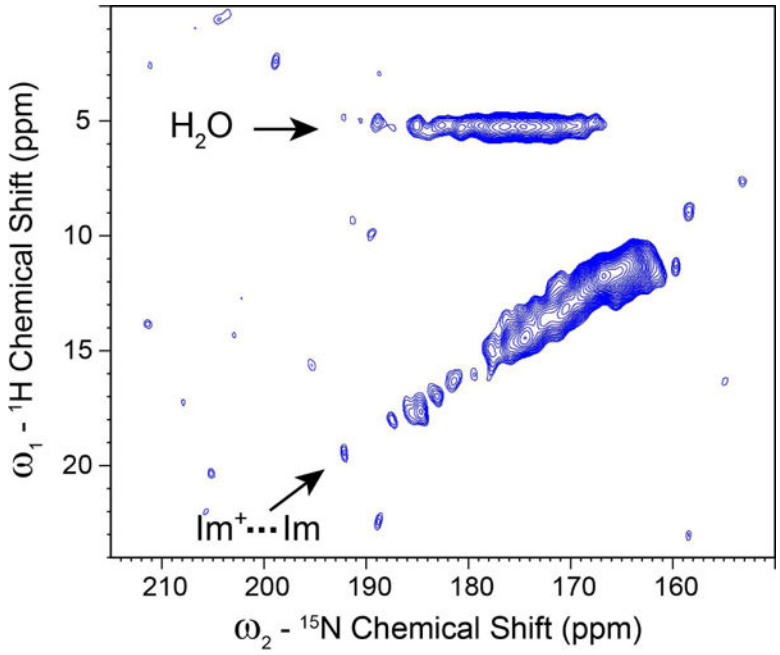

Figure 5.
2D ^{1}H-^{15}N HETCOR spectrum of the His37-labeled M2FL (pH 5.8) in DOPC/DOPE liposomes at −10°C.

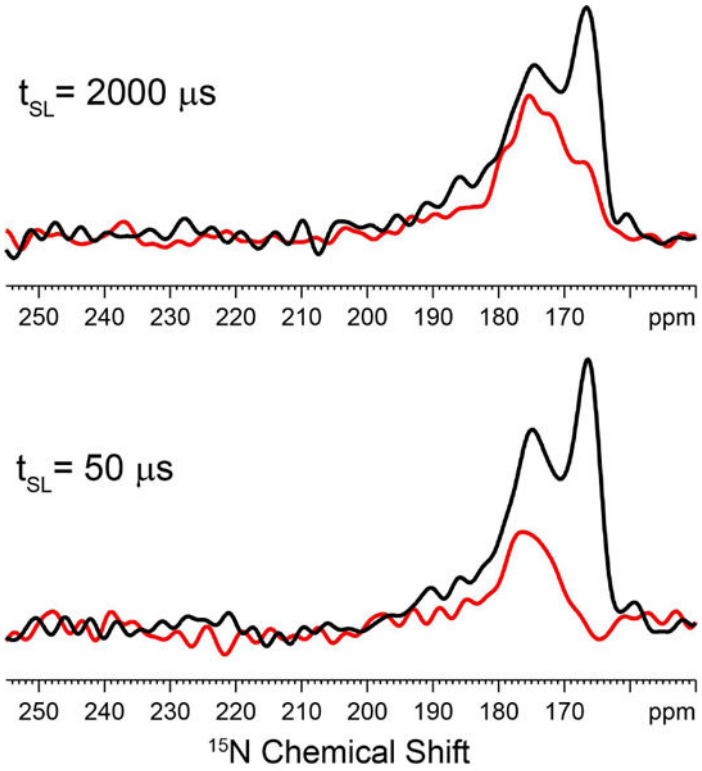

Figure 6.

Expanded ^{15}N spectra of the His37-labeled M2FL (pH 5.8) in lipid bilayers at −10°C without (black) and with (red) ^{15}N-dipolar dephasing and spinlock time t_{SL} of 50 and 2000 μs.

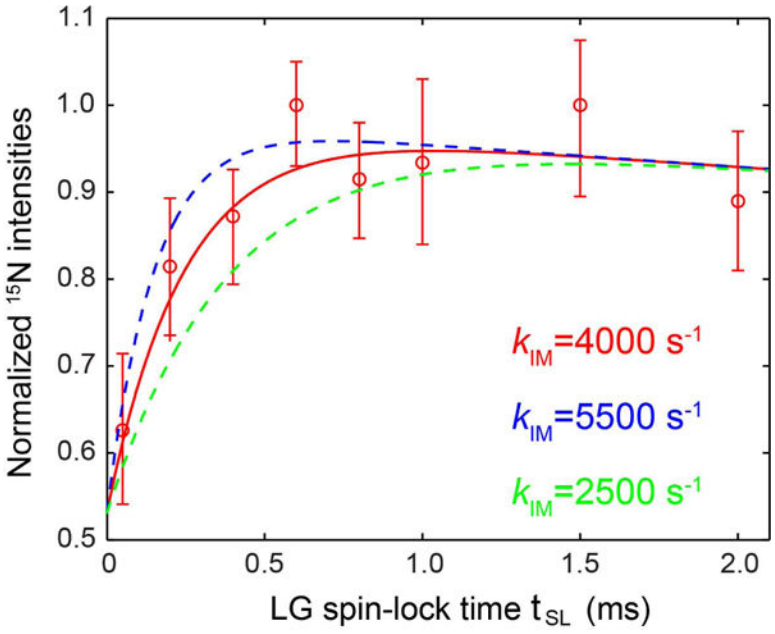

Figure 7.

Normalized dipolar-dephased ^{15}N integral intensities as a function of t_{SL} for the His37-labeled M2FL (pH 5.8) at −10°C. The red line represents the best fit curve with k_{IM}=4000 s^{-1}. The dashed green and blue lines are the curves for k_{IM}=2500 and 5500 s^{-1}, respectively.

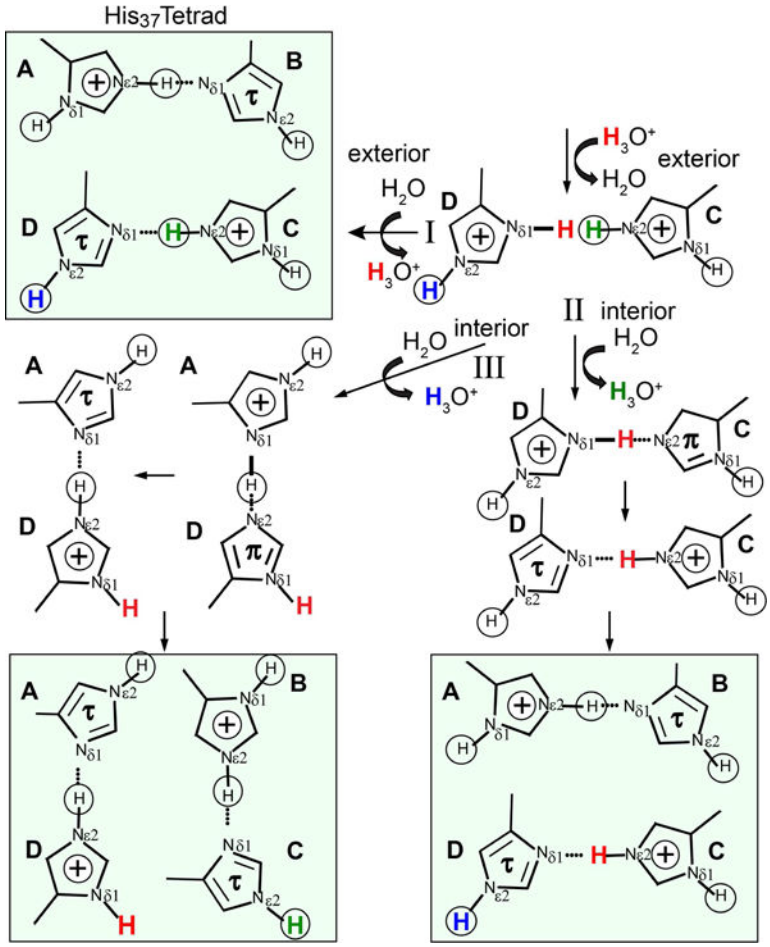

Figure 8.

Chemical exchange model between hydronium ions and the protons in the His37 NH bonds. In the upper left is the +2 state of the His tetrad. The addition of a second charge to a His pair protonating the Nδ1 site from an external water breaks an imidazole-imidazolium hydrogen bond. Three paths are identified from this point. I) returns the Nδ1 proton to waters of the external environment. II) An Nε2 proton is given up to water from the interior resulting in conductance and requiring a proton transfer from the Nδ1 to Nε2 site. III) The other Nε2 gives up its proton to water resulting in a rearrangement of the imidazolium-imidazole pairs.

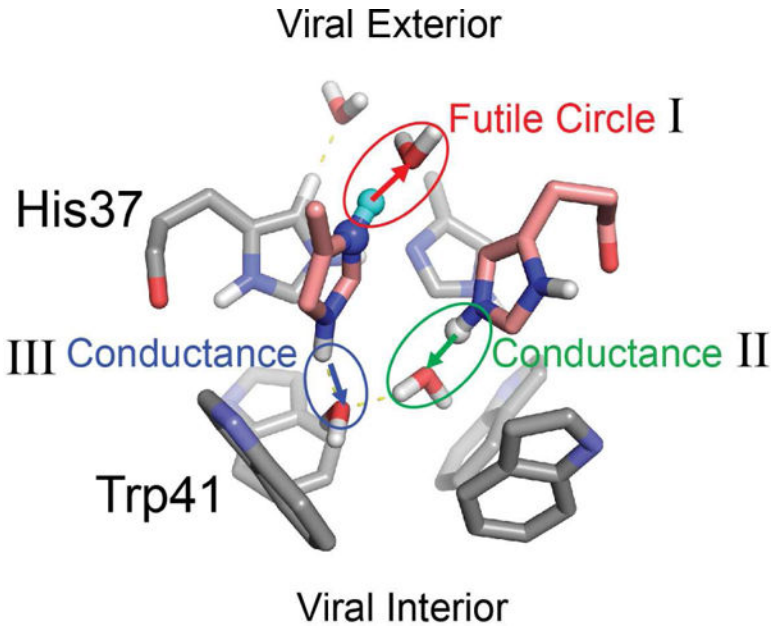

Figure 9.

Illustration of the His37 and Trp41 sidechain orientations upon the breaking of the imidazole-imidazolium hydrogen bond between a His37 C-D pair in the M2 proton channel. The paths given by numerals I, II, and III are the same as in Figure 8 and the arrows are used to illustrate the proton releasing paths.